PERGAMON

International Journal of Solids and Structures 38 (2001) 261–287

INTERNATIONAL JOURNAL OF SOLIDS and STRUCTURES

www.elsevier.com/locate/ijsolstr

Deformable body impact: dynamic plastic behaviour of a moving free–free beam striking the tip of a cantilever beam

T.X. Yu [a,*], J.L. Yang [b], S.R. Reid [c]

[a] *Department of Mechanical Engineering, Hong Kong University of Science and Technology, Clear Water Bay, Kowloon, Hong Kong*
[b] *The Solid Mechanics Research Centre, Beijing University of Aeronautics and Astronautics, Beijing 100083, People's Republic of China*
[c] *Department of Mechanical Engineering, UMIST, P.O. Box 88, Manchester M60 1QD, UK*

Received 16 March 1999; in revised form 17 November 1999

Abstract

A theoretical model based on the rigid, perfectly plastic material idealization is proposed to simulate the dynamic behaviour of two deformable beams colliding with each other. The mid-point of a moving free–free beam is assumed to impinge on the tip of a cantilever beam with the beam axes perpendicular to each other. Complete solutions are obtained for various deformation mechanisms during the dynamic response process for the two deformed beams, and plastic shear sliding is taken into account. Attention is focused on the partitioning of the input energy between the two deformed beams after impact. A deformation map in a governing parameter plane is constructed to permit the calculation of the energy partitioning for a range of the beams' parameters. This consists of nine regions corresponding to various deformation mechanisms. Typical numerical results are presented to demonstrate the influence of structural and geometrical parameters such as the ratios of the fully plastic bending moments of the two beams, of their fully plastic shear forces, of their masses per unit length and their length, on the energy partitioning after impact. Finally, the severance limit is given for the case of both beams having rectangular cross-sections. This indicates that shear sliding failure may happen in either of the beams if the initial kinetic energy is sufficiently large.

Keywords: Collision; Two deformable beams; Energy partitioning; Deformation map

1. Introduction

Over the last 50 years, the rigid, perfectly plastic material model has been widely adopted to study the dynamic behaviour of structures subjected to intense dynamic loading. By neglecting the elasticity and strain-hardening of the material, this idealization significantly simplifies the deformation mechanism of the structure without losing the key features of its dynamic response. Symonds (1967) and Symonds and Frye (1988) have shown that this idealization is applicable if the input energy is much larger than the maximum

* Corresponding author. Tel.: +852-2358-6962; fax: +852-2358-1543.
E-mail address: metxyu@usthk.ust.hk (T.X. Yu).

0020-7683/00/$ - see front matter
PII: S0020-7683(00)00019-6

elastic energy that can be stored in the structure and if the duration of the applied pulse is shorter than the fundamental period of the elastic vibration of the structure. Generally speaking, a complete solution for the structural response to impact/pulse loading can be obtained from a series of dynamically admissible deformation mechanisms of the structure. These satisfy the equations of motion, the force boundary conditions and do not violate the yield criterion at any point in the structure. This kind of complete solution provides a better estimation of the overall response, including the permanent deformation and the distribution of the dissipated energy in the structure, compared with that predicted by a mode approach (Stronge and Yu, 1993).

A review of the studies in this field indicates that almost all the previous studies deal only with the following cases: (a) where the magnitude, duration and pulse shape of the external loading applied to the structure are specified, e.g. step loading or a rectangular pulse; (b) where the magnitude and the distribution of an initial velocity field applied to the structure are specified; or (c) where the structure is subjected to impact by a rigid mass moving at a given initial velocity. It is evident, therefore, that none of these cases has considered the collision between two deformable structures. The article by Stronge and Shu (1989) considered interacting multi-component beam structures, but these structural components were connected and loaded rather than colliding with each other.

Impact between two deformable bodies or more specifically between two deformable structures could occur in various engineering scenarios and is of practical interest. For instance, a dropped beam could impinge on another beam when a space truss is being erected or collapses, or a whipping pipe could impinge on another pipe following a pipe–whip incident in a nuclear or chemical plant (Reid et al., 1998). In all cases, the colliding components are both deformable. Qualitatively similar behaviour occurs when an automobile crashes into a roadside parapet or strikes another vehicle.

In an attempt to analyse this kind of problem one needs to consider whether or not the classical rigid, perfectly plastic approach (RPPA) can still be applied to the collision between two deformable structures. By employing the RPPA in studying the title problem, i.e. that of a moving free–free beam striking the tip of a cantilever beam, this article is aimed at demonstrating the applicability of the RPPA as a simple but powerful tool for this new category of structural impact problems.

2. Theoretical model

2.1. Deformation mechanisms during the initial shear sliding phase

Consider a horizontal free–free beam of uniform cross-section moving in a vertical plane with an initial transverse speed, V_0. Assume that at time $t = 0$ the mid-point of this free–free beam strikes the tip of a cantilever beam of uniform cross-section. When the collision occurs, both the beams are in a horizontal plane and perpendicular to each other and the initial velocity of the free–free beam is normal to this plane, as indicated in Fig. 1.

As shown in Fig. 1, contact will occur at the mid-point of the free–free beam, A, and the free tip of the cantilever beam, A′. It is further assumed that during the following dynamic response of the system after impact, the free–free beam remains adhered to the tip of the cantilever beam until its initial kinetic energy has been entirely dissipated by the plastic deformations of the two beams.

Two of the earliest models for beam impact should be mentioned here, viz. that proposed by Parkes (1955) for a rigid, perfectly plastic cantilever beam subjected to impact by a rigid moving mass at its tip and that presented by Lee and Symonds (1952) for a rigid, perfectly plastic free–free beam subjected to a triangular pulse at its mid-span.

According to the deformation mechanism suggested by Parkes (1955), a travelling plastic hinge will initiate at the tip of the cantilever when the rigid moving mass suddenly strikes the tip if no limitation is

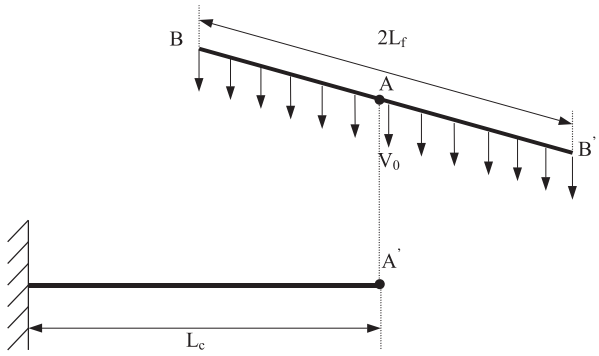

Fig. 1. A horizontal free–free beam moving in a vertical plane strikes the tip of a horizontal cantilever beam which was perpendicular to the free–free beam before impact.

imposed on the transverse shear force generated in the beam. The subsequent deformation mechanism consists of a travelling plastic hinge, which moves along the beam until it reaches the clamped root. This plastic hinge then remains stationary at the root until the rest of the kinetic energy of the system has been dissipated.

Similarly, according to the modes proposed by Lee and Symonds (1952), the deformation mechanism of a free–free beam in the transient phase contains a stationary plastic hinge at the mid-span and two travelling plastic hinges moving away from it. When the travelling hinges cease to move and vanish, the transient stage ends and then each half of the beam rotates about the central stationary hinge as rigid bodies and the central hinge dissipates the rest of the kinetic energy.

It should be noted that both Parkes (1955) and Lee and Symonds (1952) in their early studies neglected the effect of finite shear strength, so that an infinitely large shear force is accommodated at $t = 0$. This defect was remedied in later studies (e.g. Karunes and Onat, 1960; Nonaka, 1967; Symonds, 1968; Liu and Jones, 1988; Stronge and Yu, 1993; Forrestal and Hanchak, 1999) of the dynamic behaviour of rigid, perfectly plastic beams in which the effect of the shear deformation was incorporated into the deformation mechanisms.

In order to establish a more reasonable model for a moving free–free beam striking a cantilever beam, the transverse shear force is limited by the fully plastic shear force of the beams in the following analysis of the transient phase of the problem represented in Fig. 1.

If the free–free beam of cross-sectional area A_f and the cantilever beam of cross-sectional area A_c, have yield shear stresses given by $\tau_{fp} = \sigma_{fp}/2$ (or $\tau_{fp} = \sigma_{fp}/\sqrt{3}$) and $\tau_{cp} = \sigma_{cp}/2$ (or $\tau_{cp} = \sigma_{cp}/\sqrt{3}$), respectively, depending upon which of the Tresca or von Mises yield criterion is used, then the fully plastic shear forces for the two beams are

$$Q_{fp} = A_f \tau_{fp}, \tag{1}$$

$$Q_{cp} = A_c \tau_{cp}, \tag{2}$$

respectively. In the following, subscripts f and c denote the free–free beam and the cantilever beam, respectively, and subscript p denotes yield values.

At the instant when the moving free–free beam strikes the tip of the cantilever beam, the impact force is so high that shear sliding first takes place in the component that has the lower fully plastic shear force. Clearly, shear sliding will first take place at the tip of the cantilever beam if

$$Q_{cp} < 2Q_{fp}. \tag{3}$$

Otherwise, shear sliding will first take place at the mid-span of the free–free beam.

For convenience in the derivations in the following sections, P_s is defined as

$$P_s = \min\left(\frac{Q_{cp}}{2}; Q_{fp}\right), \tag{4}$$

and

$$q_s = \frac{P_s L_f}{M_{fp}}, \quad \gamma = \frac{M_{cp}}{M_{fp}}, \quad \eta_{cf} = \frac{L_c}{L_f}, \quad \beta = \frac{m_c}{m_f}, \tag{5}$$

where M_{fp} and M_{cp} are the fully plastic bending moments; L_c, the length of the cantilever; L_f, the half-length of the free–free beam; and m_f and m_c are the masses per unit length of the free–free beam and the cantilever beam, respectively. Which beam is subjected to shear sliding at the impact region determines whether P_s is equal to $Q_{cp}/2$ or Q_{fp}.

The next step in the analysis is to construct the bending deformation mechanisms for both beams during the shear sliding phase. According to the analysis given by Lee and Symonds (1952), for the free–free beam there are three possible deformation mechanisms. If $q_s < 2$, no plastic hinge appears in the free–free beam, so it moves as a rigid body. If $2 < q_s < 11.4$, a plastic hinge forms at the mid-section and both halves of the beam rotate about the hinge. If $q_s > 11.4$, a three-hinge mechanism forms, in which one hinge is at the mid-section while the other two hinges locate at a distance $\leqslant 0.404 L_f$ on both sides of the mid-section.

There are three possible deformation mechanisms for the cantilever beam. If $q_s < \frac{1}{2}\gamma/\eta_{cf}$, no plastic hinge appears in the beam and it remains stationary except that shear sliding is allowed to appear at the free tip. If $\frac{1}{2}\gamma/\eta_{cf} < q_s < \frac{3}{2}\gamma/\eta_{cf}$, a plastic hinge forms at the clamped root and the beam rotates about the root as a rigid body. If $\frac{3}{2}\gamma/\eta_{cf} < q_s$, a plastic hinge forms within the beam at a distance less than L_c from the tip, the segment between the tip and the hinge rotates about the hinge, whilst the other segment between the root and the hinge remains stationary.

The above analysis can be summarized by a map in the $q_s \sim \gamma/\eta$ plane as shown in Fig. 2. The map consists of nine regions corresponding to different deformation mechanisms during the plastic shear sliding phase. These are

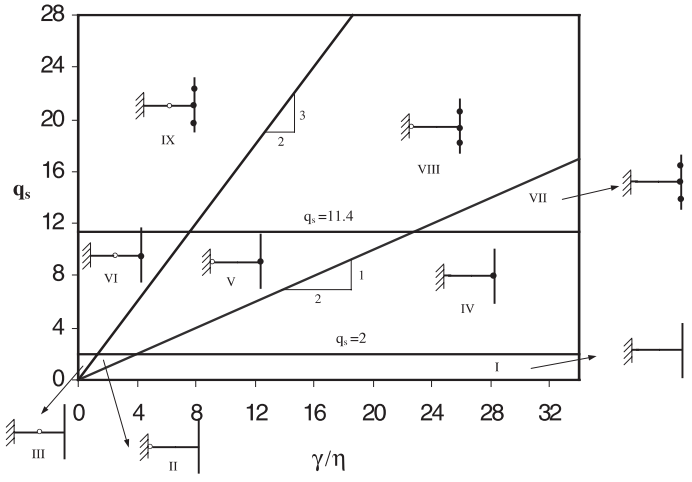

Fig. 2. A map on the q_s–γ/η plane, showing nine regions corresponding to various deformation mechanisms during the plastic shear sliding phase. The solid and hollow dots appearing in the sketches of deformation mechanisms represent the plastic hinges in the free–free beam and the cantilever beam, respectively.

Region I: $q_s < 2$ and $q_s < \gamma/2\eta_{cf}$, no plastic hinge appears in either beam.
Region II: $q_s < 2$ and $\gamma/2\eta_{cf} < q_s < 3\gamma/2\eta_{cf}$, a single plastic hinge forms at the root of the cantilever beam.
Region III: $q_s < 2$ and $3\gamma/2\eta_{cf} < q_s$, a single plastic hinge forms at an internal cross-section of the cantilever beam.
Region IV: $2 < q_s < 11.4$ and $q_s < \gamma/2\eta_{cf}$, a single plastic hinge forms at the mid-section of the free–free beam.
Region V: $2 < q_s < 11.4$ and $\gamma/2\eta_{cf} < q_s < 3\gamma/2\eta_{cf}$, two plastic hinges appear, one of which forms at the root of the cantilever beam and the other one forms at the mid-section of the free–free beam.
Region VI: $2 < q_s < 11.4$ and $3\gamma/2\eta_{cf} < q_s$, two plastic hinges appear, one of which forms at an internal cross-section of the cantilever beam and the other one forms at the mid-section of the free–free beam.
Region VII: $q_s > 11.4$ and $q_s < \gamma/2\eta_{cf}$, three plastic hinges appear, one of which forms at the mid-section of the free–free beam and the other two form at both sides of the mid-section.
Region VIII: $q_s > 11.4$ and $\gamma/2\eta_{cf} < q_s < 3\gamma/2\eta_{cf}$, four plastic hinges appear, one of which forms at the root of the cantilever beam and the other three form in the free–free beam.
Region IX: $q_s > 11.4$ and $3\gamma/2\eta_{cf} < q_s$, four plastic hinges appear, one of which forms at an internal cross-section of the cantilever beam and the other three form in the free–free beam.

Each of these regions gives a particular deformation mechanism in the initial, shear sliding phase, which greatly affects the development of the succeeding deformation process after the shear sliding phase ceases. Consequently, the final partitioning of the input energy between the cantilever beam and the free–free beam is also significantly different, which is a key point of this study.

2.2. Analysis of the entire response process for region IX

It is clear from Fig. 2 that, although nine deformation mechanisms are possible, Region IX is the most general and complicated response mechanism among them. It will be noted in the following section that the development of the deformation starting from Region IX will experience most of the deformation mechanisms related to the other regions shown in Fig. 2. Therefore, the derivation of the governing equations concentrates on Region IX. The equations relevant to other regions are given briefly in Appendix A.

2.2.1. Phase I: shear sliding phase ($0 < t < t_I$)

For the free–free beam, the velocity diagram in half of the beam (outside the shear band) is as shown in Fig. 3(a), where $\dot{W}_0, \dot{\theta}$, and $\dot{\phi}$ denote the velocity of the outer parts of the beam just outside the possible shear band around the contact point A, the angular velocity of segment AH and that of HB relative to AH, respectively. $x_h = \mathrm{AH}$ is the distance of the hinge H from the impact point. Since shear force P_s remains constant in this phase, the travelling plastic hinge speed $\dot{x}_h = 0$. As a result, the equations of motion for half of the beam are

$$-P_s = m_f\left(\ddot{W}_0 x_h + \frac{\ddot{\theta}x_h^2}{2}\right), \tag{6a}$$

$$-2M_{fp} = m_f\left(\frac{\ddot{W}_0 x_h^2}{2} + \frac{x_h^2\ddot{\theta}}{3}\right), \tag{6b}$$

$$\ddot{W}_0 + x_h\ddot{\theta} + \frac{(L - x_h)\ddot{\phi}}{2} = 0, \tag{6c}$$

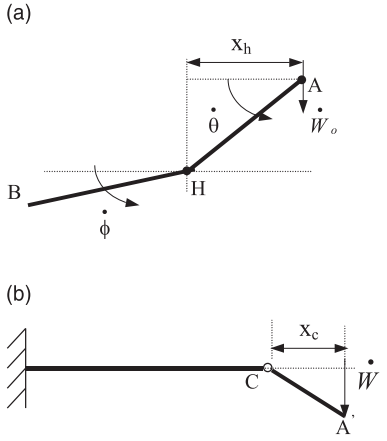

Fig. 3. Deformation mechanisms in Phase I (shear sliding phase): (a) for the free–free beam and (b) for the cantilever beam.

$$\frac{m_f(L-x_h)^2(\ddot{W}_0+x_h\ddot{\theta})}{2}+\frac{m_f(L-x_h)^3\ddot{\phi}}{3}=M_{fp}, \tag{6d}$$

where m_f is the mass per unit length of the free–free beam. For convenience, the equations are re-written in terms of non-dimensional variables defined as follows:

$$\xi_h=x_h/L_f,\quad \zeta_0=W_0/L_f,\quad \tau=t\sqrt{\frac{M_{fp}}{m_fL_f^3}},\quad \overset{\circ}{()}=d()/d\tau. \tag{7}$$

Thus, Eqs. (6a)–(6d) are re-cast as

$$\overset{\circ\circ}{\zeta}_0\xi_h+\frac{\xi_h^2\overset{\circ\circ}{\theta}}{2}=-q_s, \tag{8a}$$

$$\xi_h^2\left(\frac{\overset{\circ\circ}{\zeta}_0}{2}+\frac{\xi_h\overset{\circ\circ}{\theta}}{3}\right)=-2, \tag{8b}$$

$$\overset{\circ\circ}{\zeta}_0+\xi_h\overset{\circ\circ}{\theta}+(1-\xi_h)\frac{\overset{\circ\circ}{\phi}}{2}=0, \tag{8c}$$

$$\tfrac{1}{2}\left(\overset{\circ\circ}{\zeta}_0+\xi_h\overset{\circ\circ}{\theta}\right)(1-\xi_h)^2+\tfrac{1}{3}(1-\xi_h)^3\overset{\circ\circ}{\phi}=1. \tag{8d}$$

The equations can be solved by expressing $\overset{\circ\circ}{\zeta}_0$, $\overset{\circ\circ}{\theta}$ and $\overset{\circ\circ}{\phi}$ in terms of ξ_h. They are given by

$$\overset{\circ\circ}{\zeta}=12\left(\frac{1}{(1-\xi_h)^2}-\frac{1}{\xi_h^2}\right), \tag{9a}$$

$$\overset{\circ\circ}{\theta}=\frac{12}{\xi_h^3}-\frac{18}{\xi_h(1-\xi_h)^2}, \tag{9b}$$

$$\overset{\circ\circ}{\phi}=\frac{12}{(1-\xi_h)^3}. \tag{9c}$$

Substituting Eqs. (9a) and (9b) into Eq. (8a), leads to a relationship between q_s and ξ_h as

$$q_s = \frac{1}{\xi_h}\left(6 - \frac{3\xi_h^2}{(1-\xi_h)^2}\right). \tag{10}$$

As it is required that $q_s \geqslant 11.4$, Eq. (10) results in

$$\xi_h \leqslant 0.404, \tag{11}$$

which is a necessary condition for Region IX.

When q_s is given, ξ_h is deduced by Eq. (10), and then $\overset{\circ\circ}{\zeta}_0$, $\overset{\circ\circ}{\theta}$ and $\overset{\circ\circ}{\phi}$ can be determined by Eq. (9). By integrating Eq. (9) with respect to τ, it is found that

$$\overset{\circ}{\zeta}_0 = \frac{12(2\xi_h - 1)}{\xi_h^2(1-\xi_h)^2}\tau + \sqrt{\lambda}, \tag{12a}$$

$$\zeta_0 = \frac{6(2\xi_h - 1)}{\xi_h^2(1-\xi_h)^2}\tau^2 + \sqrt{\lambda}\tau, \tag{12b}$$

$$\overset{\circ}{\theta} = \left\{\frac{12}{\xi_h^3} - \frac{18}{\xi_h(1-\xi_h)^2}\right\}\tau, \tag{12c}$$

$$\theta = \left\{\frac{6}{\xi_h^3} - \frac{9}{\xi_h(1-\xi_h)^2}\right\}\tau^2, \tag{12d}$$

$$\overset{\circ}{\phi} = \frac{12}{(1-\xi_h)^3}\tau, \tag{12e}$$

$$\phi = \frac{6}{(1-\xi_h)^3}\tau^2, \tag{12f}$$

where

$$\lambda = \frac{m_f L_f V_0^2}{M_{fp}} \tag{13}$$

represents the non-dimensional input energy, i.e. the non-dimensional initial kinetic energy carried by the moving free–free beam.

On the other hand, for the cantilever beam, the velocity diagram outside the possible shear band is as shown in Fig. 3(b), where $\dot{W}$ and x_c denote the velocity just outside the possible shear band close to the tip of the cantilever beam and the distance between the plastic hinge and the tip, respectively, during the shear sliding phase. It is evident that as long as the localized shear deformation occurs either in the free–free beam or in the cantilever beam, we always have $\dot{W} \neq \dot{W}_0$ during the shear sliding phase.

By noting that $\dot{x}_c = 0$, because the shear force P_s remains constant, the equations of motion for the cantilever beam are

$$2P_s = \frac{1}{2}m_c\frac{d}{dt}(\dot{W}x_c), \tag{14a}$$

$$M_{cp} = \frac{1}{6}m_c\frac{d}{dt}(\dot{W}x_c^2). \tag{14b}$$

The non-dimensional forms of above equations are

$$2q_s = \frac{\beta}{2}\frac{d}{d\tau}(\dot{\zeta}\xi_c) = \frac{\beta\ddot{\zeta}\xi_c}{2}, \tag{15a}$$

$$\gamma = \frac{\beta}{6}\frac{d}{d\tau}(\dot{\zeta}\xi_c^2) = \frac{\beta\ddot{\zeta}\xi_c^2}{6}, \tag{15b}$$

where $\zeta = W/L_f$, $\xi_c = x_c/L_f$. Eliminating $\ddot{\zeta}$ from the above equations results in

$$\xi_c = \frac{3\gamma}{2q_s}. \tag{16}$$

Since it is required that

$$q_s \geqslant \frac{3\gamma}{2\eta_{cf}}, \tag{17}$$

we have

$$\xi_c \leqslant \eta_{cf}. \tag{18}$$

Substituting Eq. (16) into Eq. (15) and integrating it with respect to τ, we have

$$\dot{\zeta} = \frac{8q_s^2}{3\gamma\beta}\tau, \tag{19a}$$

$$\zeta = \frac{4q_s^2}{3\gamma\beta}\tau^2. \tag{19b}$$

The shear sliding phase terminates when $\dot{\zeta} = \dot{\zeta}_0$, and by considering Eqs. (19a) and (12a), the non-dimensional time when shear sliding ends is found to be

$$\tau_I = \sqrt{\lambda}\Big/\left[\frac{8q_s^2}{3\gamma\beta} + \frac{12(1-2\xi_h)}{\xi_h^2(1-\xi_h)^2}\right]. \tag{20}$$

Substituting Eq. (20) into Eqs. (12) and (19), $\zeta_0, \dot{\zeta}_0, \theta, \dot{\theta}, \phi, \dot{\phi}, \zeta$, and $\dot{\zeta}$ can be obtained at the end of the shear sliding phase, $\tau = \tau_I$, and are defined as $\zeta_{0I}, \dot{\zeta}_{0I}, \theta_I, \dot{\theta}_I, \phi_I, \dot{\phi}_I, \zeta_I$, and $\dot{\zeta}_I$.

The shear deformation at the impact cross-section between the cantilever beam and the free–free beam is given by

$$\Delta\zeta_I = \zeta_{0I} - \zeta_I. \tag{21}$$

The fraction of the total input kinetic energy absorbed in plastic shear sliding is approximately

$$\frac{E_s}{E_{in}} = \frac{2q_s\Delta\zeta_I}{\lambda} = \frac{3q_s\gamma\beta\xi_h^2(1-\xi_h)^2}{4[2q_s^2\xi_h^2(1-\xi_h)^2 + 9\gamma\beta(1-2\xi_h)]}. \tag{22}$$

2.2.2. Phase II: double travelling hinge phase ($t_I < t < t_{II}$)

As soon as $\dot{\zeta} = \dot{\zeta}_0$, the impact force, $2P$, in the contact area between the cantilever and the free–free beam will reduce sharply. The plastic hinges H and H′ (symmetric hinge to H on the right hand part of beam) in the free–free beam and C in the cantilever beam become travelling hinges moving away from the impact point A.

For the free–free beam, the equations of motion for segment AH are

$$-P = m_{\mathrm{f}}\left(\ddot{W}x_{\mathrm{h}} + \frac{x_{\mathrm{h}}^2\ddot{\theta}}{2}\right), \tag{23}$$

$$-2M_{\mathrm{f}p} = m_{\mathrm{f}}\left(\frac{\ddot{W}x_{\mathrm{h}}^2}{2} + \frac{x_{\mathrm{h}}^3\ddot{\theta}}{3}\right), \tag{24}$$

and for segment BH, they are

$$\ddot{W} + x_{\mathrm{h}}\ddot{\theta} + \dot{x}_{\mathrm{h}}\dot{\theta} + \frac{(L_{\mathrm{f}} - x_{\mathrm{h}})\ddot{\phi}}{2} - \dot{x}_{\mathrm{h}}\dot{\phi} = 0, \tag{25}$$

$$\frac{m_{\mathrm{f}}(L_{\mathrm{f}} - x_{\mathrm{h}})^2}{2}\left(\ddot{W} + x_{\mathrm{h}}\ddot{\theta} + \dot{x}_{\mathrm{h}}\dot{\theta} - \dot{x}_{\mathrm{h}}\dot{\phi}\right) + \frac{m_{\mathrm{f}}(L_{\mathrm{f}} - x_{\mathrm{h}})^3}{3}\ddot{\phi} = M_{\mathrm{f}p}. \tag{26}$$

For the cantilever beam, the equations of motion for segment AC are

$$2P = \tfrac{1}{2}m_{\mathrm{c}}(\ddot{W}x_{\mathrm{c}} + \dot{W}\dot{x}_{\mathrm{c}}), \tag{27}$$

$$M_{\mathrm{c}p} = \tfrac{1}{6}m_{\mathrm{c}}(\ddot{W}x_{\mathrm{c}}^2 + 2\dot{W}\dot{x}_{\mathrm{c}}x_{\mathrm{c}}). \tag{28}$$

Eliminating P from Eqs. (23) and (27) and re-arranging Eqs. (21)–(26) in their non-dimensional forms, we have

$$4\overset{\circ\circ}{\zeta}\xi_{\mathrm{h}} + 2\xi_{\mathrm{h}}^2\overset{\circ\circ}{\theta} + \beta(\overset{\circ\circ}{\zeta}\xi_{\mathrm{c}} + \overset{\circ}{\xi}_{\mathrm{c}}\overset{\circ}{\zeta}) = 0, \tag{29a}$$

$$\tfrac{1}{2}\overset{\circ\circ}{\zeta}\xi_{\mathrm{h}}^2 + \tfrac{1}{3}\overset{\circ\circ}{\theta}\xi_{\mathrm{h}}^3 + 2 = 0, \tag{29b}$$

$$\overset{\circ\circ}{\zeta} + \xi_{\mathrm{h}}\overset{\circ\circ}{\theta} + \overset{\circ}{\xi}_{\mathrm{h}}\overset{\circ}{\theta} + \frac{(1 - \xi_{\mathrm{h}})}{2}\overset{\circ\circ}{\phi} - \overset{\circ}{\xi}_{\mathrm{h}}\overset{\circ}{\phi} = 0, \tag{29c}$$

$$\frac{(1 - \xi_{\mathrm{h}})^2}{2}\left(\overset{\circ\circ}{\zeta} + \xi_{\mathrm{h}}\overset{\circ\circ}{\theta} + \overset{\circ}{\xi}_{\mathrm{h}}\overset{\circ}{\theta} - \overset{\circ}{\xi}_{\mathrm{h}}\overset{\circ}{\phi}\right) + \frac{(1 - \xi_{\mathrm{h}})^3}{3}\overset{\circ\circ}{\phi} = 1, \tag{29d}$$

$$\overset{\circ\circ}{\zeta}\xi_{\mathrm{c}}^2 + 2\overset{\circ}{\zeta}\overset{\circ}{\xi}_{\mathrm{c}}\xi_{\mathrm{c}} = \frac{6\gamma}{\beta}. \tag{29e}$$

Eqs. (29) can be put into convenient forms for numerical calculations by expressing $\overset{\circ\circ}{\zeta}$, $\overset{\circ\circ}{\theta}$, $\overset{\circ\circ}{\phi}$, $\overset{\circ}{\xi}_{\mathrm{h}}$ and $\overset{\circ}{\xi}_{\mathrm{c}}$ in terms of ξ_{h} and ξ_{c}, resulting in

$$\overset{\circ\circ}{\zeta} = \frac{6}{\xi_{\mathrm{c}}}\left\{\frac{\gamma}{\beta\xi_{\mathrm{c}}} - \frac{2\left(\gamma + \frac{\gamma\xi_{\mathrm{h}}}{\beta\xi_{\mathrm{c}}} - \frac{2\xi_{\mathrm{c}}}{\xi_{\mathrm{h}}}\right)}{\beta\xi_{\mathrm{c}} + 2\xi_{\mathrm{h}}}\right\}, \tag{30a}$$

$$\overset{\circ\circ}{\theta} = -\frac{3}{\xi_{\mathrm{h}}^3}\left\{2 + \left(\frac{\xi_{\mathrm{h}}}{\xi_{\mathrm{c}}}\right)^2\left[\frac{3\gamma}{\beta} - \frac{6(\gamma + \frac{\gamma\xi_{\mathrm{h}}}{\beta\xi_{\mathrm{c}}} - \frac{2\xi_{\mathrm{c}}}{\xi_{\mathrm{h}}})}{\beta + 2\xi_{\mathrm{h}}/\xi_{\mathrm{c}}}\right]\right\}, \tag{30b}$$

$$\overset{\circ\circ}{\phi} = \frac{12}{(1-\xi_h)^3}, \tag{30c}$$

$$\overset{\circ}{\xi}_h = \left(\frac{1}{\overset{\circ}{\theta}-\overset{\circ}{\phi}}\right)\left[\frac{6}{\xi_h^2}+\frac{3\gamma}{\beta\xi_c^2}-\frac{6}{(1-\xi_h)^2}-\frac{6(\gamma+\frac{\gamma\xi_h}{\beta\xi_c}-\frac{2\xi_c}{\xi_h})}{\xi_c(\beta\xi_c+2\xi_h)}\right], \tag{30d}$$

$$\overset{\circ}{\xi}_c = \frac{6(\gamma+\frac{\gamma\xi_h}{\beta\xi_c}-\frac{2\xi_c}{\xi_h})}{\overset{\circ}{\zeta}(\beta\xi_c+2\xi_h)}. \tag{30e}$$

The initial conditions for Phase II, which come from the state when Phase I terminates, are given by

$$\begin{aligned}
&\zeta|_{\tau=\tau_I} = \zeta_I, \qquad \overset{\circ}{\zeta}\Big|_{\tau=\tau_I} = \overset{\circ}{\zeta}_I,\\
&\theta|_{\tau=\tau_I} = \theta_I, \qquad \overset{\circ}{\theta}\Big|_{\tau=\tau_I} = \overset{\circ}{\theta}_I,\\
&\phi|_{\tau=\tau_I} = \phi_I, \qquad \overset{\circ}{\phi}\Big|_{\tau=\tau_I} = \overset{\circ}{\phi}_I,\\
&\xi_h|_{\tau=\tau_I} = \text{given from Eq. (10)},\\
&\xi_c|_{\tau=\tau_I} = \frac{3\gamma}{2q_s}.
\end{aligned} \tag{31}$$

Eqs. (30a)–(30e) together with the initial condition (31) can be solved using a Runge-Kutta procedure. As the response develops, the travelling plastic hinge, C, in the cantilever beam approaches the clamped root whilst the travelling plastic hinges, H and H′, on the either side of the mid-point of the free–free beam move more and more slowly as the difference between the relative angular velocities $\overset{\circ}{\theta}$ and $\overset{\circ}{\phi}$ reduces. Therefore, in each calculation step it is necessary to check the following two conditions:

Condition (i): whether or not the plastic travelling hinge in the cantilever beam, C, has arrived at the clamped root in the cantilever beam, i.e. whether $\xi_c = \eta_{cf}$;

Condition (ii): whether or not the speeds of the plastic travelling hinges in the free–free beam, H and H′, become zero, i.e. $\overset{\circ}{\xi}_h = 0$ (or $\overset{\circ}{\theta}-\overset{\circ}{\phi}=0$).

When Phase II ends depends upon, which one of these two conditions is first satisfied. If Condition (i) is satisfied before Condition (ii), then the travelling hinge, C, will become stationary at the root of the cantilever beam while the H and H′ hinges are still travelling along the free–free beam until their speed becomes zero during the succeeding response (i.e. in Phase III). On the contrary, if Condition (ii) is satisfied before Condition (i), then the travelling hinges H and H′ will vanish and the two halves of the free–free beam rotate about the stationary hinge at the mid-section, whilst the travelling hinge, C, is still moving to the root of the cantilever beam until it arrives there during the succeeding response (i.e. in Phase III).

Accordingly, Phase III will be analysed for these two different cases as follows.

2.2.3. Phase III ($t_{II} < t < t_{III}$), if Condition (i) is satisfied before Condition (ii)

As soon as $\xi_c = \eta_{cf}$, the travelling hinge, C, reaches and remains at the root of the cantilever beam. Thus, the cantilever beam rotates about the stationary root hinge as a rigid body in the following phases of the

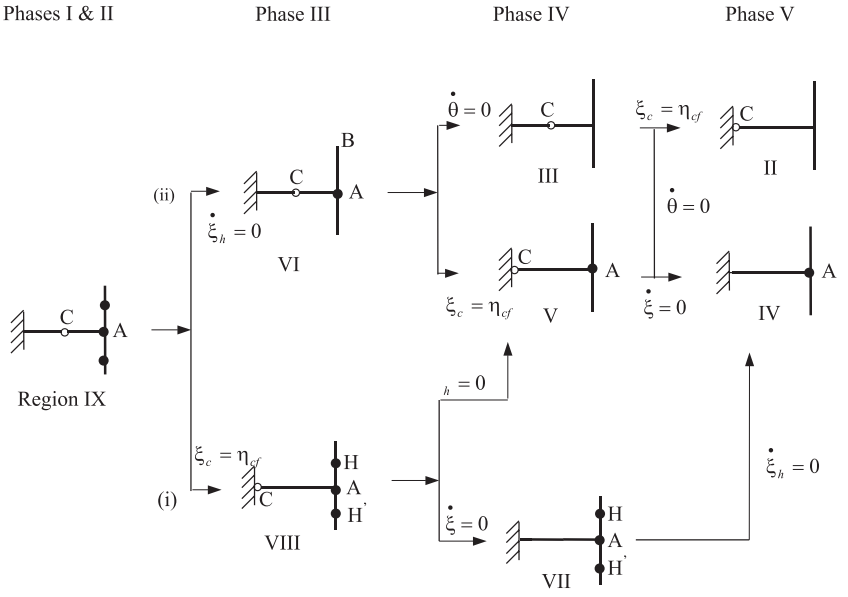

Fig. 4. Evolution of the deformation mechanisms in the case starting from a shear sliding phase located in Region IX. The solid and hollow dots appearing in the sketches of deformation mechanisms represent the plastic hinges in the free–free beam and in the cantilever beam, respectively.

response. The deformation mechanism is as shown in the lower half of Fig. 4. The equations of motion given by Eqs. (23)–(26) for the free–free beam are still valid, while for the cantilever beam the non-dimensional equation of motion is given by

$$2PL_{\mathrm{c}} - M_{cp} = \frac{\ddot{W} m_{\mathrm{c}} L_{\mathrm{c}}^2}{3}. \tag{32}$$

Eliminating P from Eqs. (21) and (29), the non-dimensional form of the equation of motion can be expressed by

$$\overset{\circ\circ}{\zeta}\left(\xi_{\mathrm{h}} + \frac{1}{6}\beta\eta_{\mathrm{cf}}\right) + \frac{\xi_{\mathrm{h}}^2\overset{\circ\circ}{\theta}}{2} + \frac{\gamma}{2\eta_{\mathrm{cf}}} = 0. \tag{33}$$

The non-dimensional Eqs. (29b)–(29d) which are the equations of motion for the free–free beam are still valid. Moreover, $\overset{\circ\circ}{\zeta}$, $\overset{\circ\circ}{\theta}$, $\overset{\circ\circ}{\phi}$, and $\overset{\circ}{\xi}_{\mathrm{h}}$ can be expressed in terms of ξ_{h} as

$$\overset{\circ\circ}{\zeta} = \frac{6(6\eta_{\mathrm{cf}} - \gamma\xi_{\mathrm{h}})}{\eta_{\mathrm{cf}}\xi_{\mathrm{h}}(2\beta\eta_{\mathrm{cf}} + 3\xi_{\mathrm{h}})}, \tag{34a}$$

$$\overset{\circ\circ}{\theta} = -\frac{6}{\xi_{\mathrm{h}}^3} - \frac{9(6\eta_{\mathrm{cf}} - \gamma\xi_{\mathrm{h}})}{\eta_{\mathrm{cf}}\xi_{\mathrm{h}}^2(2\beta\eta_{\mathrm{cf}} + 3\xi_{\mathrm{h}})}, \tag{34b}$$

$$\overset{\circ}{\xi}_{\mathrm{h}}(\overset{\circ}{\theta} - \overset{\circ}{\phi}) = \left(\frac{6}{\xi_{\mathrm{h}}^2} - \frac{6}{(1-\xi_{\mathrm{h}})^2} + \frac{3(6\eta_{\mathrm{cf}} - \gamma\xi_{\mathrm{h}})}{\eta_{\mathrm{cf}}\xi_{\mathrm{h}}(2\beta\eta_{\mathrm{cf}} + 3\xi_{\mathrm{h}})}\right), \tag{34c}$$

$$\overset{\circ\circ}{\phi} = \frac{12}{(1-\xi_h)^3}. \tag{34d}$$

The initial conditions, which come from the state when Phase II terminates, are given by

$$\begin{aligned}
&\zeta|_{\tau=\tau_{II}} = \zeta_{II}, \qquad \overset{\circ}{\zeta}\Big|_{\tau=\tau_{II}} = \overset{\circ}{\zeta}_{II},\\
&\theta|_{\tau=\tau_{II}} = \theta_{II}, \qquad \overset{\circ}{\theta}\Big|_{\tau=\tau_{II}} = \overset{\circ}{\theta}_{II},\\
&\phi|_{\tau=\tau_{II}} = \phi_{II}, \qquad \overset{\circ}{\phi}\Big|_{\tau=\tau_{II}} = \overset{\circ}{\phi}_{II},\\
&\xi_h|_{\tau=\tau_{II}} = \xi_{hII}.
\end{aligned} \tag{35}$$

When Phase III terminates depends upon, whether, $\overset{\circ}{\xi}_h = 0$ or $\overset{\circ}{\zeta} = 0$.

If $\overset{\circ}{\xi}_h = 0$ at the end of Phase III, then from Eq. (34c) we have

$$\left(\frac{6}{\xi_h^2} - \frac{6}{(1-\xi_h)^2} + \frac{3(6\eta_{cf} - \gamma\xi_h)}{\eta_{cf}\xi_h(2\beta\eta_{cf} + 3\xi_h)}\right) = 0, \tag{36}$$

which gives the limiting position of the travelling hinge when it vanishes in the free–free beam. After that, the response enters Phase IV in which stationary hinge mechanisms exist in both beams. One hinge is at the root of the cantilever beam and the other locates at the mid-section of the free–free beam. The rest of the kinetic energy of the system will be dissipated by these two stationary hinges. A detailed analysis of Phase IV for this response mechanism is given below.

If $\overset{\circ}{\zeta} = 0$ at the end of Phase III, the motion of the cantilever beam ceases and it remains stationary in the following phase. The rest of the kinetic energy of the system will be dissipated by the three plastic hinges in the free–free beam, i.e. one stationary hinge, A, at the mid-section and two travelling hinges, H and H′, on both the sides of the mid-section of the free–free beam (Lee and Symonds, 1952).

2.2.4. Phase III ($t_{II} < t < t_{III}$), if Condition (ii) is satisfied before Condition (i)

When the speed of the plastic travelling hinges, H and H′, becomes zero in the free–free beam, i.e. $\overset{\circ}{\xi}_h = 0$ (or $\overset{\circ}{\theta} - \overset{\circ}{\phi} = 0$), the beam deforms in a single-hinge mechanism with a stationary hinge at A whilst the travelling hinge, C, in the cantilever beam is still moving towards the root. By noting that Eqs. (30a) and (30e) are still valid and considering the moments taken about A, for the rigid segment BA, we have

$$-M_{fp} = m_f\left(\frac{\ddot{W}L_f^2}{2} + \frac{\ddot{\theta}L_f^3}{3}\right), \tag{37}$$

which in the non-dimensional form is given by

$$\frac{\overset{\circ\circ}{\zeta}}{2} + \frac{1}{3}\overset{\circ\circ}{\theta} = -1. \tag{38}$$

Further, $\overset{\circ\circ}{\zeta}$, $\overset{\circ\circ}{\theta}$ and $\overset{\circ}{\xi}_c$ can be expressed in terms of ξ_c as

$$\overset{\circ\circ}{\zeta} = \frac{12\xi_c - 6\gamma}{\xi_c(2+\beta\xi_c)}, \tag{39}$$

$$\overset{\circ\circ}{\theta} = -3 - \frac{18\xi_c - 9\gamma}{\xi_c(2+\beta\xi_c)}, \tag{40}$$

$$\overset{\circ}{\xi}_c = \frac{1}{\overset{\circ}{\zeta}}\left(\frac{3\gamma}{\beta\xi_c} - \frac{6\xi_c - 3\gamma}{(2+\beta\xi_c)}\right). \tag{41}$$

The initial conditions of Phase III, which come from the state when Phase II terminates, are given in Eq. (35).

Phase III ends when the travelling hinge in the cantilever beam arrives at the root of the beam, i.e. $\xi_c = \eta_{cf}$. Then, the response enters Phase IV in which stationary hinge mechanisms are formed in both beams. One hinge is at the root of the cantilever beam and the other locates at the mid-section of the free–free beam.

2.2.5. Phase IV: two stationary hinges ($t_{III} < t < t_{IV}$)

Since the cantilever beam rotates about its root hinge and the free–free beam rotates about its mid-section as rigid bodies, the equations of motion in non-dimensional form are given by (a detailed derivation can be found in Appendix A, see Region V)

$$2q\eta_{cf} - \gamma = \tfrac{1}{3}\overset{\circ\circ}{\zeta}\beta\eta_{cf}^2, \tag{42}$$

$$-q = \overset{\circ\circ}{\zeta} + \frac{\overset{\circ\circ}{\theta}}{2}, \tag{43}$$

$$-1 = \frac{\overset{\circ\circ}{\zeta}}{2} + \frac{\overset{\circ\circ}{\theta}}{3}. \tag{44}$$

After eliminating q from the above equations, $\overset{\circ\circ}{\zeta}$ and $\overset{\circ\circ}{\theta}$ can be expressed by

$$\overset{\circ\circ}{\zeta} = \frac{6(3\eta_{cf} - \gamma)}{\eta_{cf}(3+2\beta\eta_{cf})}, \tag{45}$$

$$\overset{\circ\circ}{\theta} = -\left[3 + \frac{9(3\eta_{cf} - \gamma)}{\eta_{cf}(3+2\beta\eta_{cf})}\right]. \tag{46}$$

Integrating the above equations with respect to τ and applying the initial conditions at the end of Phase III, we have

$$\overset{\circ}{\zeta} = \frac{6(3\eta_{cf} - \gamma)}{\eta_{cf}(3+2\beta\eta_{cf})}\tau + \overset{\circ}{\zeta}_{III}, \tag{47}$$

$$\zeta = \frac{3(3\eta_{cf} - \gamma)}{\eta_{cf}(3+2\beta\eta_{cf})}\tau^2 + \overset{\circ}{\zeta}_{III}\tau + \zeta_{III}, \tag{48}$$

$$\overset{\circ}{\theta} = -\left[3 + \frac{9(3\eta_{cf} - \gamma)}{\eta_{cf}(3+2\beta\eta_{cf})}\right]\tau + \overset{\circ}{\theta}_{III}, \tag{49}$$

$$\theta = -\frac{1}{2}\left[3 + \frac{9(3\eta_{cf} - \gamma)}{\eta_{cf}(3+2\beta\eta_{cf})}\right]\tau^2 + \overset{\circ}{\theta}_{III}\tau + \theta_{III}. \tag{50}$$

When Phase IV terminates depends upon, whether $\overset{\circ}{\zeta} = 0$ or $\overset{\circ}{\theta} = 0$. Firstly, consider the case when $\overset{\circ}{\zeta} = 0$. From Eq. (43), it is found that

$$(\tau_{IV})_1 = \frac{\overset{\circ}{\zeta}_{III}\eta_{cf}(3 + 2\beta\eta_{cf})}{6(\gamma - 3\eta_{cf})}. \tag{51}$$

On the other hand, if $\overset{\circ}{\theta} = 0$ it follows from Eq. (45) that

$$(\tau_{IV})_2 = \frac{\overset{\circ}{\theta}_{III}\eta_{cf}(3 + 2\beta\eta_{cf})}{36\eta_{cf} + 6\beta\eta_{cf}^2 - 9\gamma}. \tag{52}$$

Eqs. (51) and (52) provide two possible times when Phase IV terminates.

2.2.6. Phase Va

If $(\tau_{IV})_1 > (\tau_{IV})_2$, which indicates that the cantilever beam ceases its motion before the free–free beam does, the following Phase V will dissipate the rest of the kinetic energy in the free–free beam through an additional rotation, $\Delta\theta_{Vf}$, at the hinge located at the mid-section. According to the equation of energy conservation, we have

$$M_{fp}\Delta\theta_{Vf} = \tfrac{1}{6}m_f L_f^3 \dot{\theta}_{IV}^2, \tag{53}$$

where $\dot{\theta}_{IV}$ is the angular velocity about the mid-section hinge when $\overset{\circ}{\zeta} = 0$.

2.2.7. Phase Vb

On the other hand, if $(\tau_{IV})_1 < (\tau_{IV})_2$, which indicates that the free–free beam ceases its motion before the cantilever beam does, the following Phase V will dissipate the rest of the kinetic energy in the cantilever beam through an additional root rotation, $\Delta\theta_{Vc}$, and energy conservation requires

$$M_{cp}\Delta\theta_{Vc} = (\tfrac{1}{6}m_c L_c + m_f L_f)\dot{W}_{IV}^2, \tag{54}$$

where $\dot{W}_{IV}$ is the vertical velocity at the tip of the cantilever beam when $\overset{\circ}{\theta} = 0$.

2.3. Energy partitioning for a cantilever beam struck by a free–free beam

An interesting issue to resolve is how much of the input kinetic energy is dissipated in the target cantilever beam and how much is dissipated in the flying free–free beam. Using the complete solutions for the dynamic response described above, together with the detailed analysis given in Appendix A combined with the deformation mechanism map shown in Fig. 2, the energy partitioning in the two beams can be obtained. This can be expressed as fractions of the initial energy dissipated in the different deformation modes.

In accordance with the regions shown in the map (Fig. 2), the following results can be established. Let E_{in}, E_s, E_c, E_f denote the input kinetic energy, the shear sliding energy, the energy dissipated in the cantilever beam and the energy dissipated in the free–free beam, respectively, during the impact response process.

Region I:

$$\frac{E_s}{E_{in}} = 1, \qquad \frac{E_c}{E_{in}} = 0, \qquad \frac{E_f}{E_{in}} = 0.$$

Region II:

$$\frac{E_s}{E_{in}}=\frac{q_s\beta\eta_{cf}^2}{q_s(\beta\eta_{cf}^2+6\eta_{cf})-3\gamma},\qquad \frac{E_c}{E_{in}}=\frac{6q_s\eta_{cf}-3\gamma}{q_s(\beta\eta_{cf}^2+6\eta_{cf})-3\gamma},\qquad \frac{E_f}{E_{in}}=0.$$

Region III:

$$\frac{E_s}{E_{in}}=\frac{\beta\eta_{cf}}{4+\beta\eta_{cf}},\qquad \frac{E_c}{E_{in}}=\frac{4}{4+\beta\eta_{cf}},\qquad \frac{E_f}{E_{in}}=0.$$

Region IV:

$$\frac{E_s}{E_{in}}=\frac{q_s}{2(2q_s-3)},\qquad \frac{E_c}{E_{in}}=0,\qquad \frac{E_f}{E_{in}}=\frac{3q_s-6}{2(2q_s-3)}.$$

Region V:

$$\frac{E_s}{E_{in}}=\frac{q_s\beta\eta_{cf}^2}{3(2q_s\eta_{cf}-\gamma)+2\beta\eta_{cf}^2(2q_s-3)},\qquad \frac{E_c}{E_{in}}=\frac{\gamma\zeta_c}{\eta_{cf}\lambda},\quad \frac{E_f}{E_{in}}=\frac{2\theta_f}{\lambda},$$

where ζ_c and θ_f are the final non-dimensional deflection at the tip of the cantilever beam and the final rotation angle at the mid-section of the free–free beam, respectively.

Region VI:

$$\frac{E_s}{E_{in}}=\frac{q_s\beta\eta_{cf}^2}{2[(2q_s-3)\beta\eta_{cf}^2+3\gamma]},\qquad \frac{E_c}{E_{in}}=\frac{\gamma(\psi_{ct}+\psi_{cs})}{\lambda},\qquad \frac{E_f}{E_{in}}=\frac{2\theta_f}{\lambda},$$

where ψ_{ct} and ψ_{cs} are, respectively, the total rotations caused by the travelling hinges as they pass through the free–free beam and the rotation angle about the stationary hinge at the root of the cantilever beam.

Region VII:

$$\frac{E_s}{E_{in}}=\frac{q_s}{12}\cdot\frac{\xi_h^2(1-\xi_h)^2}{(1-2\xi_h)},\qquad \frac{E_c}{E_{in}}=0,\qquad \frac{E_f}{E_{in}}=\frac{2(\theta_{II}-\phi_{II})+2\theta_f}{\lambda}.$$

Region VIII:

$$\frac{E_s}{E_{in}}=\frac{q_s\beta\eta_{cf}^2\xi_h^2(1-\xi_h)^2}{12\beta\eta_{cf}^2(1-2\xi_h)+3\xi_h^2(1-\xi_h)^2(2q_s\eta_{cf}-\gamma)},$$

$$\frac{E_c}{E_{in}}=\frac{\gamma\zeta_c}{\eta_{cf}\lambda},\qquad \frac{E_f}{E_{in}}=\frac{2(\theta_{II}-\phi_{II})+2\theta_f}{\lambda}\ \text{ or }\ \frac{E_f}{E_{in}}=\frac{2(\theta_{III}-\phi_{III})+2\theta_f}{\lambda}.$$

Region IX:

$$\frac{E_s}{E_{in}}=\frac{3q_s\gamma\beta\xi_h^2(1-\xi_h)^2}{4[2q_s^2\xi_h^2(1-\xi_h)^2+9\gamma\beta(1-2\xi_h)]},$$

$$\frac{E_c}{E_{in}}=\frac{\gamma(\psi_{ct}+\psi_{cs})}{\lambda},$$

$$\frac{E_f}{E_{in}}=\frac{2\theta_f+2(\theta_{II}-\phi_{II})}{\lambda}\ \text{ or }\ \frac{E_f}{E_{in}}=\frac{2(\theta_{III}-\phi_{III})+2\theta_f}{\lambda}$$

$$\text{or }\ \frac{E_f}{E_{in}}=\frac{2(\theta_{IV}-\phi_{IV})+2\theta_f}{\lambda}.$$

3. Typical examples and discussion

3.1. Example 1: a cantilever beam of rectangular cross-section struck by a moving free–free beam of rectangular cross-section

It is assumed that both beams are made of the same material and the cross-sections of both beams are rectangular with the same width b and depths h_c and h_f for the cantilever beam and the free–free beam, respectively. Other geometrical parameters are selected to be

$$L_f/h_f = 30, \qquad \eta_{cf} = L_c/L_f = 1$$

so that the half-length of the free–free beam is 30 times its depth and is equal to the total length of the cantilever beam. The structural parameters are given by

$$\gamma = \frac{M_{cp}}{M_{fp}} = \left(\frac{h_c}{h_f}\right)^2, \qquad \beta = \frac{h_c}{h_f}.$$

When $h_c < 2h_f$, the plastic shear sliding will take place at the tip of the cantilever beam during an early stage of the response. Explicitly,

$$q_s = \frac{L_f}{h_f}\frac{h_c}{h_f} = 30\frac{h_c}{h_f}.$$

When $h_c > 2h_f$, the plastic shear sliding will take place on the mid-section of the free–free beam during the early stage and we have

$$q_s = \frac{2L_f}{h_f} = 60.$$

Fig. 5 shows the partitioning of the input energy between the two beams for both the cases. It is observed that more than 98% of the total input energy will be dissipated in the cantilever beam when $h_c/h_f < 1$, in

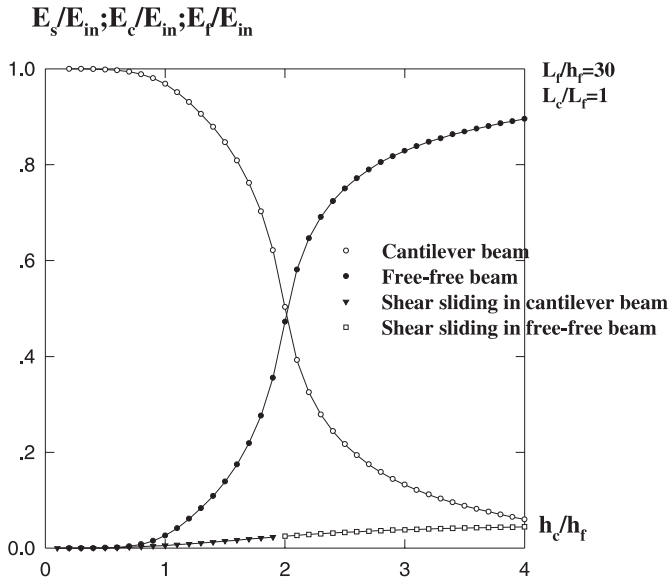

Fig. 5. The energy partitioning of the input energy E_{in} between the two beams of rectangular cross-section.

which the maximum sliding energy is about 0.4% of the total energy and is dissipated in the cantilever beam. With the increase of the ratio h_c/h_f, the energy dissipated in the free–free beam increases sharply. At $h_c/h_f = 3$, most of the input energy (about 80%) will be dissipated by the free–free beam, while the cantilever beam only dissipates 18% of the input energy.

3.2. Example 2: a cantilever beam of solid circular cross-section struck by a moving free–free beam of solid circular cross-section

It is again assumed that both beams are made of the same material and the half-length of the free–free beam is equal to the total length of the cantilever beam (i.e. $\eta_{cf} = 1$). The radius of the cross-section is R_f for the free–free beam and R_c for the cantilever beam, and $L_f/R_f = 30$ is taken. Since $M_{fp} = 4\sigma_P R_f^3/3$ and $M_{cp} = 4\sigma_P R_c^3/3$, where σ_P denotes the yield stress of the material, we have

$$\gamma = \frac{M_{cp}}{M_{fp}} = \left(\frac{R_c}{R_f}\right)^3, \qquad \beta = \frac{m_c}{m_f} = \left(\frac{R_c}{R_f}\right)^2.$$

By using Eq. (2), it is found that when $R_c < \sqrt{2}R_f$, the plastic shear sliding will take place at the tip of the cantilever beam during the early stage of the response, and

$$q_s = \frac{3\pi}{16}\frac{L_f}{R_f}\left(\frac{R_c}{R_f}\right)^2 = 17.67\left(\frac{R_c}{R_f}\right)^2.$$

On the other hand, when $R_c > \sqrt{2}R_f$, the plastic shear sliding will take place at the mid-section of the free–free beam during the early stage of the response, and

$$q_s = \frac{3\pi}{8}\frac{L_f}{R_f} = 35.34.$$

Fig. 6 shows the partitioning of the input energy between the two beams. It is observed that more than 98% of the total input energy will be dissipated in the cantilever beam when $R_c/R_f < 1$, in which the maximum sliding energy is about 1% of the total energy and is dissipated in the cantilever beam. With the increase of the ratio R_c/R_f from 1 to 2, a great part of the energy dissipation transfers from the cantilever beam to the free–free beam. At $R_c/R_f = 2$, only 10% of the input energy will be dissipated by the cantilever beam and the rest of the input energy (about 90%) will be dissipated by the free–free beam, about 8% being as the result of shear sliding.

3.3. The effects of the length ratio, η_{cf}, on the energy partitioning

If both the cantilever beam and the free–free beam have the same cross-sectional geometry and mechanical behaviour, the influence of the length ratio, η_{cf}, on the energy partitioning between two beams is of importance. Fig. 7(a)–(c) shows the energy partitioning of the input energy between the two beams, when the length ratio, η_{cf}, changes from 0.01 to 0.5, while values of $\gamma = 1$, $\beta = 1$ and $q_s = 20, 60, 150$ are taken. It is observed that more than 98% of the total input energy is dissipated by the cantilever beam if $\eta_{cf} > 0.3$, which is independent of the magnitude of q_s. Even for a very short cantilever beam such as $0.1 < \eta_{cf} < 0.3$, at least 30% of the input energy is dissipated by the cantilever beam. Therefore, for a target cantilever beam with the same geometrical and mechanical parameters as that of the flying free–free beam, the length ratio

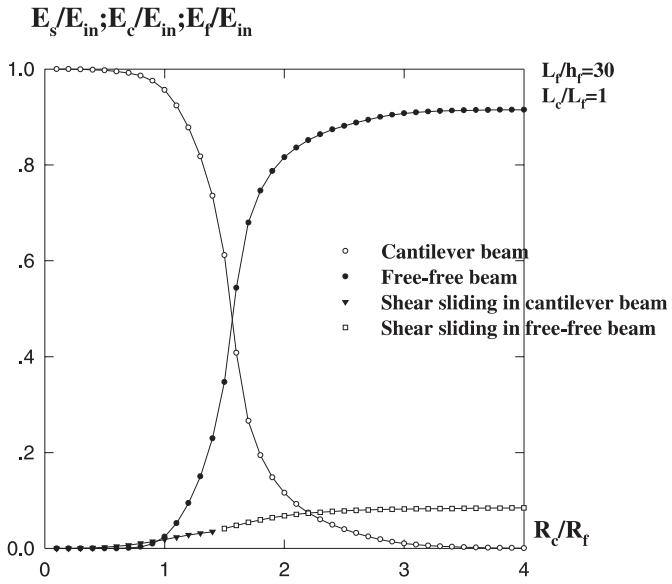

Fig. 6. The energy partitioning of the input energy E_{in} between the two beams of solid circular cross-section.

equal to 0.3 is a critical value, beyond which most of the input energy (about 98%) will be trapped by the target cantilever beam.

3.4. The effects of the fully plastic bending moment ratio, γ, on the energy partitioning

The fully plastic bending moment ratio, γ, is one of the important parameters to significantly influence the energy partitioning between the target and driving beams. Fig. 8(a)–(c) shows the energy partitioning for the total input energy versus the fully plastic bending moment ratio, γ, when $\beta = 1, \eta_{cf} = 1$ and values of $q_s = 6, 20$ and 60 are taken. It is observed from Fig. 8 that there is a critical point at $\gamma = 5$. In the neighbourhood of this point the behaviour of the energy partitioning between the target beam and driving beam undergoes a remarkable change, i.e. most of the input energy will be dissipated by the target cantilever beam when $\gamma < 5$, while most of the input energy will be dissipated by the driving free–free beam when $\gamma > 5$. According to Fig. 8, it is clear that this characteristic is approximately independent of q_s. On the other hand, it can also be seen from Fig. 8 that, with the decrease of q_s, the proportion of shear sliding energy dissipated increases. It should be noted from Fig. 8(a) that in the case of $q_s = 6$, when $\gamma \geqslant 12$ the cantilever target beam does not dissipate any energy since $q_s < 0.5\gamma/\beta$ which belongs to Regions I and IV, as shown in Fig. 2.

3.5. The effects of the mass ratio, β, on the energy partitioning

Fig. 9 shows the energy partitioning versus the mass ratio, β, when values of $R = 1, \eta_{cf} = 1$ and $q_s = 20$ are taken. It is observed that with the increase of β, the plastic shear sliding energy also increases but approaches a constant (14% of the total energy). When $\beta = 30$, the energy dissipated in the target cantilever beam will decrease to 25% of the total input energy and that in the driving free–free beam will increase to 61%.

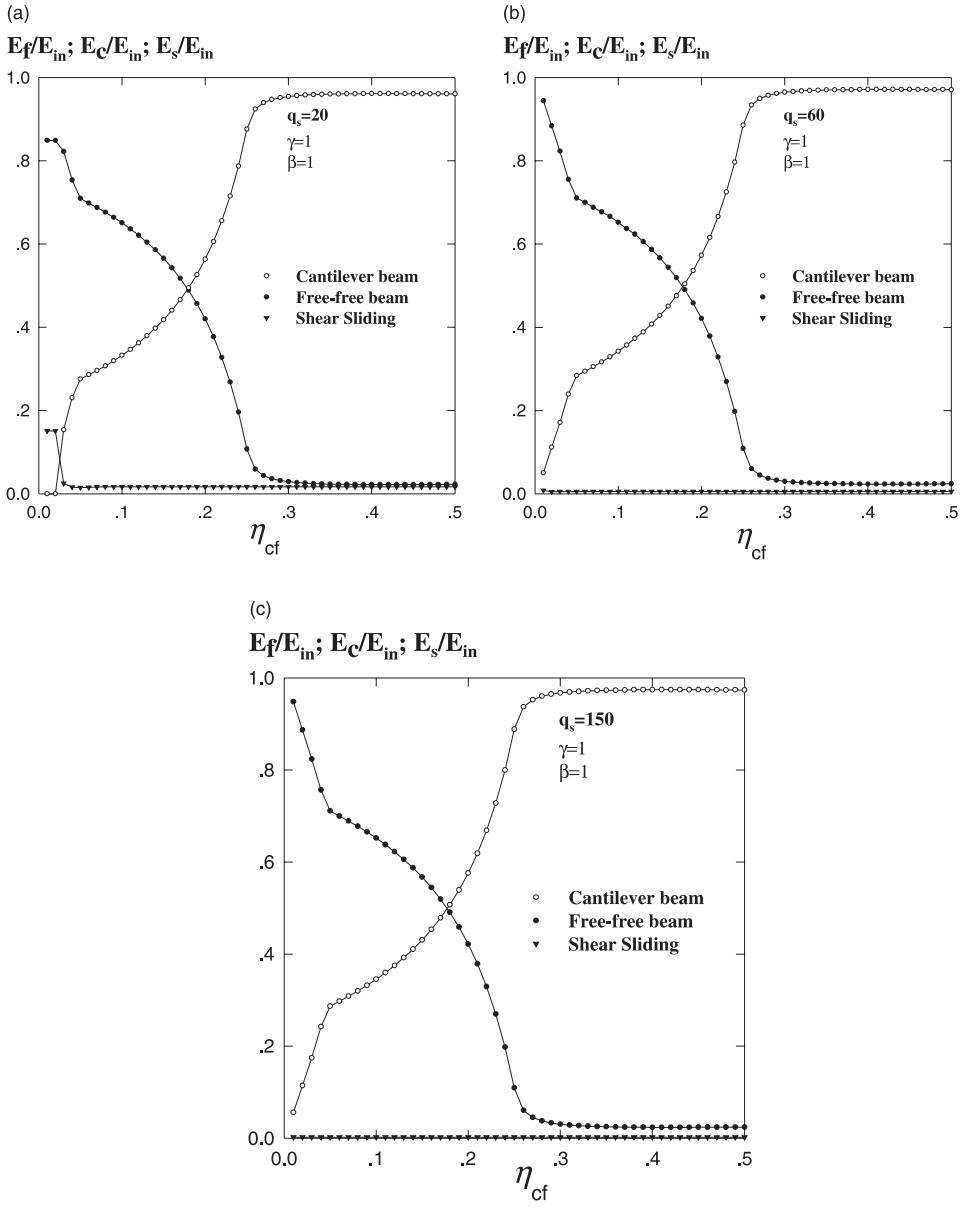

Fig. 7. The influence of the length ratio $\eta_{cf} = L_c/L_f$ on the energy partitioning of the input energy E_{in} between the two beams: (a) $q_s = 20, \gamma = 1$ and $\beta = 1$; (b) $q_s = 60, \gamma = 1$ and $\beta = 1$ and (c) $q_s = 150, \gamma = 1$ and $\beta = 1$.

4. Severance limit

As seen in Section 2.2, in the dynamic response process after the collision of a free–free beam on a cantilever beam, the first phase is a shear sliding phase. This is the case for all the parameter regions discussed above. Obviously, if during Phase I, the shear sliding displacement in the free–free beam or in the

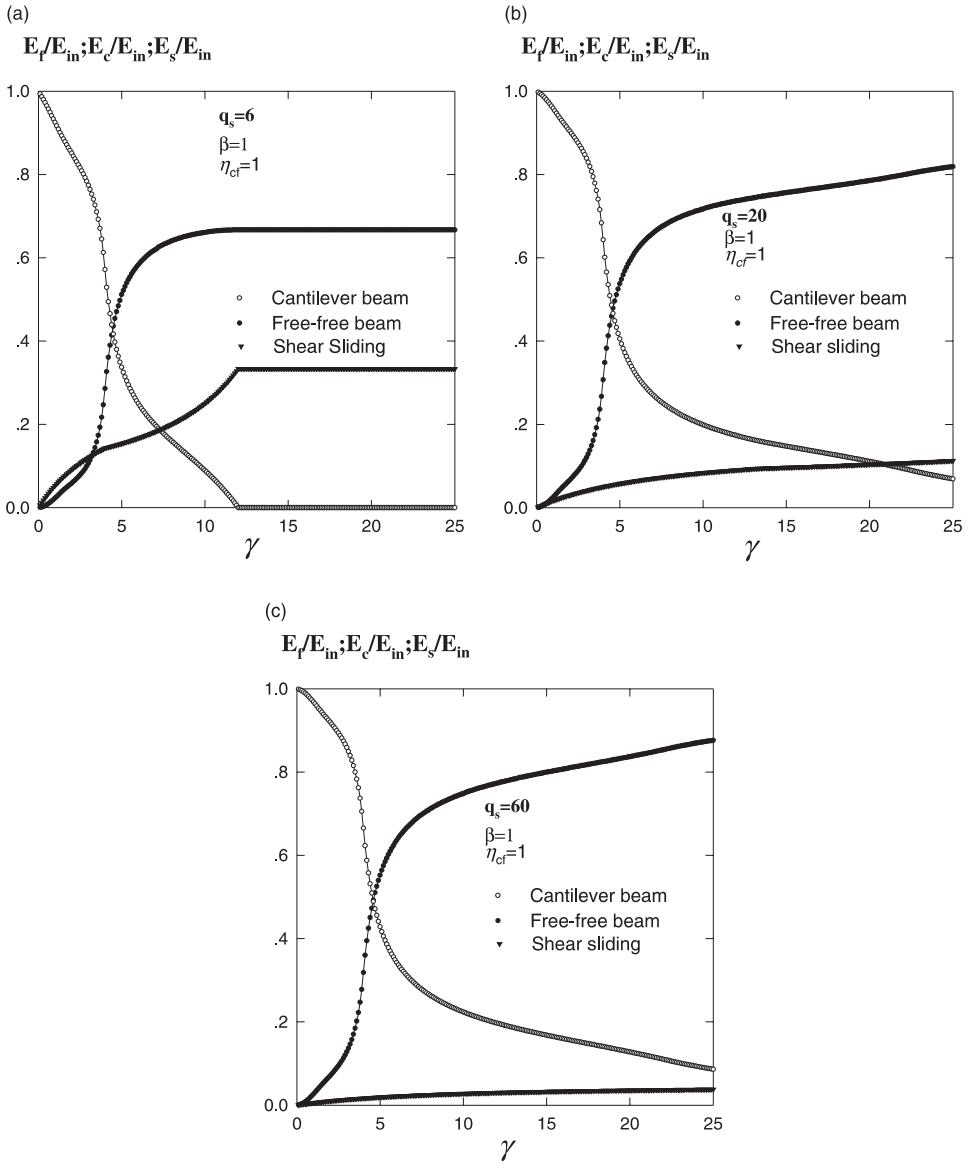

Fig. 8. The influence of the fully plastic bending moment ratio $\gamma = M_{cp}/M_{fp}$ on the energy partitioning of the input energy E_{in} between the two beams: (a) $q_s = 6, \eta_{cf} = 1$ and $\beta = 1$; (b) $q_s = 20, \eta_{cf} = 1$ and $\beta = 1$; (c) $q_s = 60, \eta_{cf} = 1$ and $\beta = 1$.

cantilever beam reaches the depth of the respective beam, a perforation or a cleavage will occur. The impact velocity for which this first occurs is termed the severance limit herein. In principle, the relevant severance limit can be determined for each of the nine regions shown in Fig. 2. However, since so many parameters are involved, no closed-form expressions for the severance limit can be obtained.

Therefore, instead of providing tedious derivations of this limit for all possible cases, we shall concentrate on a special case, viz. Example 1 (Section 3.1), in which both the cantilever beam and free–free beam have rectangular cross-sections. As in Example 1, both beams are assumed to have the same width, b, but

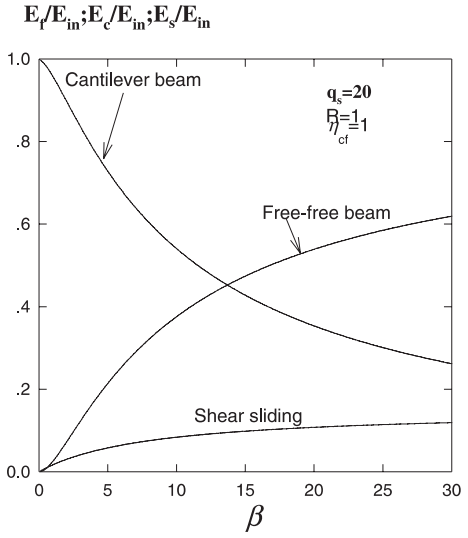

Fig. 9. The energy partitioning versus the mass ratio $\beta = m_c/m_f, q_s = 20, \eta_{cf} = 1$ and $R = 1$.

different depths, h_c and h_f, respectively. The total sliding displacement during Phase 1 can be calculated from Eqs. (22), (A.5), (A.8), (A.16), (A.18), (A.20), (A.25) and (A.27).

Analysis of the above example indicates that severance may happen at the tip region of the cantilever beam if $h_c/h_f < 2$, or it may happen at the middle of the free–free beam if $h_c/h_f > 2$. Whether it occurs or not depends on the initial kinetic energy of the moving free–free beam, that is

$$K_{f0} = \frac{1}{2} m_f (2L_f) V_0^2 = m_f L_f V_0^2 \tag{55}$$

which can be non-dimensionized using the fully plastic bending moment of the free–free beam as

$$\lambda = K_{f0}/M_{fp} = m_f L_f V_0^2 / M_{fp}. \tag{56}$$

Accordingly, the severance limit can be depicted in the plane of parameters h_c/h_f and λ.

For the cases of $L_c/L_f = 1, L_f/L_f = 30$ and 10, the severance limits are represented by the solid lines in Fig. 10(a) and (b), respectively. In each figure, the solid line divides the parameter plane into three regions: severance in the cantilever beam, severance in the free–free beam and no severance. Thus, these figures can also be regarded as shear failure maps.

It is seen from Fig. 10 that shear failure is most unlikely to happen when the depth ratio h_c/h_f is smaller than but close to 2. This is because within this range of depth ratio, the resistances of both beams to the shear sliding are almost identical, so higher energy is required to produce severance in one of them (i.e. the cantilever beam in this case).

5. Concluding remarks

In this first attempt to analyse the dynamic behaviour of two deformable beams colliding with each other, the rigid, perfectly plastic material idealization has been employed to obtain complete solutions for their dynamic response and to explore the various deformation mechanisms involving plastic shear sliding

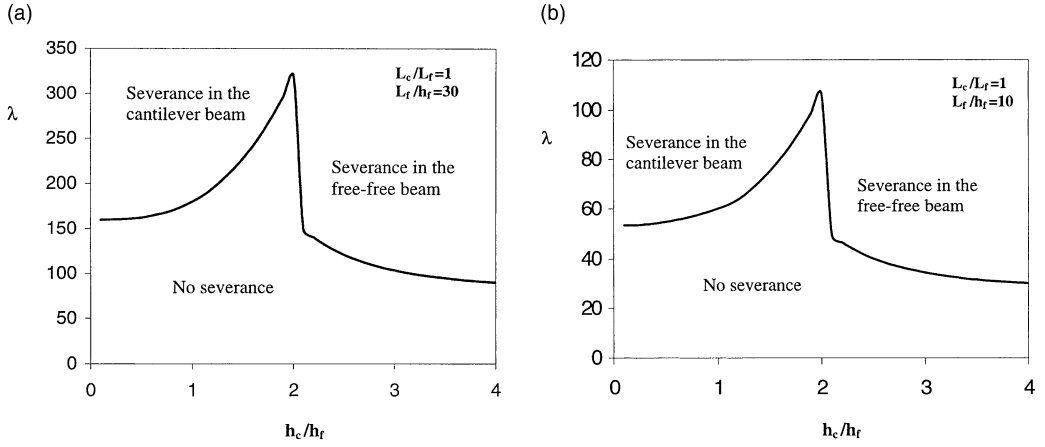

Fig. 10. A shear failure map showing the severance limits of the beams: (a) $\eta_{cf} = L_c/L_f = 1$ and $L_f/h_f = 30$ and (b) $\eta_{cf} = L_c/L_f = 1$ and $L_f/h_f = 10$.

and travelling or stationary plastic hinges. Particular attention has been paid to the partitioning of the input energy between the two deformed beams after impact.

Typical numerical results have demonstrated that structural and geometrical parameters, such as the ratio of the fully plastic bending moments of the beams, the relative magnitudes of the fully plastic shear forces, the masses per unit length and the lengths of the beams, all have significant influences on the energy partitioning. Finally, the severance limit has been calculated for the case when both beams have rectangular cross-sections, indicating that shear sliding failure may happen in either of the beams if the initial kinetic energy is sufficiently large.

It can be seen from the present analysis that, because of the coupling of the two beams through their common interaction force and contact point deflection, their deformations consist of much more complicated combinations of mechanisms compared with those for a beam struck by a rigid projectile, even within the rigid, perfectly plastic idealization which greatly simplifies the deformation patterns. It is evident that these idealized deformation mechanisms and the relevant failure modes should be further verified by experiments and elastic–plastic finite element (or finite difference) analyses, similar to those performed by the authors for cantilever beams (Reid and Gui, 1987; Yu, 1993) or free–free beams under local impact (Yu et al., 1996).

Acknowledgements

The work described in this article was supported financially by grant number JSR98/31 under the UK/Hong Kong Joint Research Scheme. The visit of the second author (JLY) to HKUST was supported by the Croucher Foundation Visitorship, which is also gratefully acknowledged. The third author (SRR) would also like to acknowledge the support of Magnox Electric plc for work on this topic.

Appendix A

The dynamic response for the regions other than Region IX (Fig. 2) is described in this appendix. Note that the derivation of the equations is the same as those in Sections 2.2 and 2.3 in this article.

A.1. Region VIII

A.1.1. Phase I: shear sliding phase ($0 < t < t_1$)

For the free–free beam, the non-dimensional Eqs. (8a)–(8d) and (12a)–(12f) are still valid, and the non-dimensional equation for the cantilever beam is

$$2q_s\eta_{cf} - \gamma = \frac{1}{3}\overset{\circ\circ}{\zeta}\beta\eta_{cf}^2. \tag{A.1}$$

Integrating the above equation with respect to τ yields

$$\overset{\circ}{\zeta} = \frac{3(2q_s\eta_{cf} - \gamma)}{\beta\eta_{cf}^2}\tau, \tag{A.2}$$

$$\zeta = \frac{3(2q_s\eta_{cf} - \gamma)}{2\beta\eta_{cf}^2}\tau^2. \tag{A.3}$$

The shear sliding phase terminates when $\overset{\circ}{\zeta} = \overset{\circ}{\zeta}_0$, and by considering Eqs. (A.2) and (12a), the non-dimensional time when shear sliding ends is found to be

$$\tau_I = \frac{\sqrt{\lambda}}{\frac{3(2q_s\eta_{cf}-\gamma)}{\beta\eta_{cf}^2} + \frac{12(1-2\xi_h)}{\xi_h^2(1-\xi_h)^2}}. \tag{A.4}$$

The shear deformation at the impact cross-section between the cantilever beam and the free–free beam is estimated by Eq. (21) and the portion of plastic shear sliding energy out of the total input kinetic energy is

$$\frac{E_s}{E_{in}} = \frac{2q_s\Delta\zeta_I}{\lambda} = \frac{q_s\beta\eta_{cf}^2\xi_h^2(1-\xi_h)^2}{12\beta\eta_{cf}^2(1-2\xi_h) + 3\xi_h^2(1-\xi_h)^2(2q_s\eta_{cf}-\gamma)}. \tag{A.5}$$

The following response phases will experience the same deformation mechanisms as those in Region IX beginning from Phase III when $\xi_c = \eta_{cf}$.

A.2. Region VII

A.2.1. Phase I: shear sliding phase ($0 < t < t_1$)

As there is no deformation in the cantilever beam during the whole response process, $\overset{\circ}{\zeta} \equiv 0$ and $\zeta \equiv 0$, and for the free–free beam the non-dimensional equations (8a)–(8d) and (12a)–(12f) are still valid. The shear sliding phase terminates when $\overset{\circ}{\zeta}_0 = 0$. From Eq. (12a), we have

$$\tau_I = \frac{\sqrt{\lambda}\xi_h^2(1-\xi_h)^2}{12(1-2\xi_h)}. \tag{A.6}$$

Substituting Eq. (A.6) into Eq. (12b), gives

$$\Delta\zeta_I = \frac{6(2\xi_h-1)\tau_I^2}{\xi_h^2(1-\xi_h)^2} + \sqrt{\lambda}\tau_I = \frac{\lambda}{24}\frac{\xi_h^2(1-\xi_h)^2}{(1-2\xi_h)}. \tag{A.7}$$

The shear deformation at the impact cross-section between the cantilever beam and the free–free beam is estimated by Eq. (21) and the portion of plastic shear sliding energy out of the total input kinetic energy is

$$\frac{E_s}{E_{in}} = \frac{2q_s\Delta\zeta_I}{\lambda} = \frac{q_s}{12}\frac{\xi_h^2(1-\xi_h)^2}{(1-2\xi_h)}. \tag{A.8}$$

Since the cantilever beam will remain stationary in the following phases, the remaining kinetic energy of the system will be dissipated by the three plastic hinges in the free–free beam, i.e. one stationary hinge, A, at the mid-section and two travelling hinges, H and H′, on both the sides of this mid-section.

A.3. Region VI

A.3.1. Phase I: shear sliding phase ($0 < t < t_I$)

For the free–free beam, the velocity diagram refers to Fig. 11. The equations of motion for the right half of the beam are

$$P_s = m_f\left(\ddot{W}_0 L_f + \frac{L_f^2}{2}\ddot{\theta}\right), \tag{A.9}$$

$$-M_{fp} = m_f\left(\frac{\ddot{W}_0 L_f^2}{2} + \frac{\ddot{\theta}L_f^3}{3}\right) \tag{A.10}$$

and their non-dimensional form of the above equations after introducing the non-dimensional variables defined in Eq. (7) are

$$-q_s = \overset{\circ\circ}{\zeta}_0 + \frac{\overset{\circ\circ}{\theta}}{2}, \tag{A.11}$$

$$-1 = \frac{\overset{\circ\circ}{\zeta}_0}{2} + \frac{\overset{\circ\circ}{\theta}}{3}. \tag{A.12}$$

Eliminating $\overset{\circ\circ}{\theta}$ from the above equations and integrating it with respect to τ, we have

$$\overset{\circ}{\zeta}_0 = (6-4q_s)\tau + \sqrt{\lambda}, \tag{A.13}$$

$$\zeta_0 = (3-2q_s)\tau^2 + \sqrt{\lambda}\tau. \tag{A.14}$$

For the cantilever beam, the non-dimensional equations of motion (15a) and (15b) are still valid and the solutions for $\overset{\circ}{\zeta}$ and ζ can be found from Eqs. (19a) and (19b). The shear sliding phase terminates when $\overset{\circ}{\zeta} = \overset{\circ}{\zeta}_0$, and by considering Eqs. (A.13) and (19a), the non-dimensional time when shear sliding ends is found to be

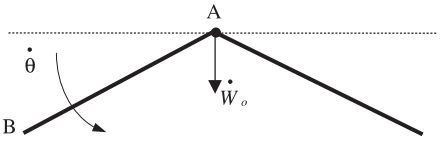

Fig. 11. The deformation mechanism of the free–free beam in Phase I for Region VI.

$$\tau_{\mathrm{I}} = \frac{\beta\xi_{\mathrm{c}}^2\sqrt{\lambda}}{(4q_{\mathrm{s}}-6)\beta\xi_{\mathrm{c}}^2+6\gamma}, \tag{A.15}$$

whilst the portion of plastic shear sliding energy out of the total input kinetic energy is

$$\frac{E_{\mathrm{s}}}{E_{\mathrm{in}}} = \frac{2q_{\mathrm{s}}\Delta\zeta_{\mathrm{I}}}{\lambda} = \frac{q_{\mathrm{s}}\beta\xi_{\mathrm{c}}^2}{2[(2q_{\mathrm{s}}-3)\beta\xi_{\mathrm{c}}^2+3\gamma]}, \tag{A.16}$$

where ξ_{c} is given by Eq. (16). The following response phases will experience the deformation mechanisms which are same as those in Region IX beginning from Phase III when $\overset{\circ}{\xi}_{\mathrm{h}} = 0$.

A.4. Region V

A.4.1. Phase I: shear sliding phase ($0 < t < t_I$)

For the free–free beam, the non-dimensional equations (A.11)–(A.14) are still valid, and for the cantilever beam its non-dimensional equation (A.1) is still valid. Following the same procedure as in the previous section, it is found that

$$\tau_{\mathrm{I}} = \frac{\sqrt{\lambda}\beta\eta_{\mathrm{cf}}^2}{3(2q_{\mathrm{s}}\eta_{\mathrm{cf}}-\gamma)+\beta\eta_{\mathrm{cf}}^2(4q_{\mathrm{s}}-6)}, \tag{A.17}$$

$$\frac{E_{\mathrm{s}}}{E_{\mathrm{in}}} = \frac{2q_{\mathrm{s}}\Delta\zeta_{\mathrm{I}}}{\lambda} = \frac{q_{\mathrm{s}}\beta\eta_{\mathrm{cf}}^2}{3(2q_{\mathrm{s}}\eta_{\mathrm{cf}}-\gamma)+2\beta\eta_{\mathrm{cf}}^2(2q_{\mathrm{s}}-3)}. \tag{A.18}$$

The following response phases will experience the deformation mechanisms which are same as those in Region IX beginning from Phase IV.

A.5. Region IV

A.5.1. Phase I: shear sliding phase ($0 < t < t_I$)

As there is no deformation in the cantilever beam during the whole response process, $\overset{\circ}{\zeta} \equiv 0$ and $\zeta \equiv 0$, and for the free–free beam the non-dimensional equations (A.11)–(A.14) are still valid. The shear sliding phase terminates when $\overset{\circ}{\zeta}_0 = 0$. From Eq. (A.13), we have

$$\tau_{\mathrm{I}} = \frac{\sqrt{\lambda}}{4q_{\mathrm{s}}-6} \tag{A.19}$$

while the portion of plastic shear sliding energy out of the total input kinetic energy is

$$\frac{E_{\mathrm{s}}}{E_{\mathrm{in}}} = \frac{2q_{\mathrm{s}}\Delta\zeta_{\mathrm{I}}}{\lambda} = \frac{q_{\mathrm{s}}}{2(2q_{\mathrm{s}}-3)}. \tag{A.20}$$

The following response phases will experience the same deformation mechanisms as those in Region IX beginning from Phase IV when $\overset{\circ}{\zeta} = 0$.

A.6. Region III

A.6.1. Phase I: shear sliding phase ($0 < t < t_I$)

For the cantilever beam, the non-dimensional equations of motion (15a) and (15b) are still valid, and for the free–free beam there is no deformation and only a sliding occurs at the impact point; therefore, the sliding is driven by

$$q_s = -\overset{\circ\circ}{\zeta}_0. \tag{A.21}$$

Integrating (A.17) with respect to τ, we have

$$\overset{\circ}{\zeta}_0 = -q_s\tau + \sqrt{\lambda}, \tag{A.22}$$

$$\zeta_0 = \frac{-q_s\tau^2}{2} + \sqrt{\lambda}\tau. \tag{A.23}$$

The shear sliding phase terminates when $\overset{\circ}{\zeta} = \overset{\circ}{\zeta}_0$, and by considering Eqs. (A.18) and (19a), the non-dimensional time when shear sliding ends is found to be

$$\tau_I = \frac{\beta\xi_c^2\sqrt{\lambda}}{q_s\beta\xi_c^2 + 6\gamma}, \tag{A.24}$$

where ξ_c is given by Eq. (16) and the portion of plastic shear sliding energy out of the total input kinetic energy is

$$\frac{E_s}{E_{in}} = \frac{2q_s\Delta\zeta_I}{\lambda} = \frac{\beta\xi_c}{4 + \beta\xi_c}. \tag{A.25}$$

The following response phases will experience the same deformation mechanisms as those in Region IX beginning from Phase IV when $\overset{\circ}{\theta} = 0$.

A.7. Region II

For the cantilever beam its non-dimensional equation (A.1) is still valid, and for the free–free beam there is no deformation and only a sliding occurs at the impact point. Therefore, the non-dimensional sliding equation (A.17) is valid. Following the same procedure as above, it is found

$$\tau_I = \frac{\beta\eta_{cf}^2\sqrt{\lambda}}{q_s(\beta\eta_{cf}^2 + 6\eta_{cf}) - 3\gamma}, \tag{A.26}$$

$$\frac{E_s}{E_{in}} = \frac{2q_s\Delta\zeta_I}{\lambda} = \frac{q_s\beta\eta_{cf}^2}{q_s(\beta\eta_{cf}^2 + 6\eta_{cf}) - 3\gamma}. \tag{A.27}$$

Since the free–free beam will remain stationary in the following phases, the remaining kinetic energy of the system will be dissipated by the plastic stationary hinges at the root of the cantilever beam.

A.8. Region I

For this particular case, both the free–free beam and the cantilever beam remain undeformed during the response process, and only shear sliding occurs at the impact point. According to the energy conservation, the initial kinetic energy will be entirely dissipated in the shear sliding phase. Thus,

$$2P_s \Delta W = \frac{1}{2} 2m_f L_f V_0^2, \tag{A.28}$$

where ΔW is the shear deformation at the impact point.

References

Forrestal, M.J., Hanchak, S.J., 1999. Perforation experiments on HY-100 steel plates with 4340 R_c 38 and maraging T-250 steel rod projectiles. Int. J. Impact Engng. 22, 923–933.

Karunes, B., Onat, E.T., 1960. On the effect of shear on plastic deformation of beams under transverse impact loading. J. Appl. Mech. 27, 107.

Lee, E.H., Symonds, P.S., 1952. Large plastic deformation of beams under transverse impact. J. Appl. Mech. 19, 308.

Liu, J.H., Jones, N., 1988. Dynamic response of a rigid clamped beam struck by a mass at any point on the span. Int. J. Solid Struct. 24, 251.

Nonaka, T., 1967. Some interaction effects in a problem of plastic beam dynamics, parts 1–3. J. Appl. Mech. 34, 623.

Parkes, E.W., 1955. The permanent deformation of a cantilever struck transversely at its tip. Proc. R. Soc. Series A 228, 462.

Reid, S.R., Gui, X.G., 1987. On the elastic–plastic deformation of cantilever beams subjected to tip impact. Int. J. Impact Engng. 6, 109–127.

Reid, S.R., Yu, T.X., Yang, J.L., 1998. An elastic–plastic hardening–softening cantilever beam subjected to a force pulse at its tip: a model for pipe whip. Proc. R. Soc. Lond. A 454, 997–1029.

Stronge, W.J., Shu, D., 1989. Coupling of dynamic plastic deformation in multi-component structures. Inst. Phys. Conf. Ser. No 102: Session 9. Paper presented at Int. Conf. Mech. Prop. Materials at High Rates of Strain, Oxford. pp. 473–480.

Stronge, W.J., Yu, T.X., 1993. Dynamic Models for Structural Plasticity. Springer, London.

Symonds, P.S., 1967. Survey of methods of analysis for plastic deformation of structure under dynamic loading. Brown. University, Division of Engineering Report BU/NSRDC/, pp. 1–67.

Symonds, P.S., 1968. Plastic shear deformations in dynamic load problems. In: Heyman, J., Leckie, F.A. (Eds.), Engineering Plasticity Cambridge Univ. Press, London, pp. 647–664.

Symonds, P.S., Frye, C.W.G., 1988. On the relation between rigid-plastic and elastic–plastic predictions of response to pulse loading. Int. J. Impact Engng. 7, 139–149.

Yu, T.X., 1993. Elastic effect in the dynamic plastic response of structures. In: Jones, N., Wierzbicki, T. (Eds.), Structural Crashworthiness and Failure. Elsevier, Amsterdam, pp. 341–384 (Chapter 9).

Yu, T.X., Yang, J.L., Reid, S.R., Austin, C.D., 1996. Dynamic behaviour of elastic–plastic free–free beam subjected to impulsive loading. Int. J. Solids Struct. 33, 2659–2680.